RSC Advances

PAPER

View Article Online
View Journal | View Issue

Check for updates

Cite this: *RSC Adv.*, 2022, **12**, 26733

Synergistic effect of graphene oxide and hydroxylated graphene on the enhanced properties of cement composites†

Yundong Pu,[a] Sen Yang,[a] Meng Qi,[b] Kuang Sheng,[a] Junfeng Bi,[a] Fukun Fan[a] and Xiaoya Yuan *[a]

Graphene oxide (GO) shows a remarkable reinforcing effect in the application of cement composite engineering while it also harms the workability of fresh cement slurry. Hydroxylated graphene (HO-G) can effectively avoid the severe adverse effects on the fluidity of cement slurry as happened in the case of GO, but the enhancement of the flexural strength of cement composites is not as good as that of GO. As such, considering the advantages and disadvantages of these two nanomaterials in cement-based composite applications, this study investigated the effect of hybrid GO/HO-G with various ratios on the macro-properties and microstructure of cement composites in comparison with that of individual GO and HO-G. The results revealed a better synergistic improvement on the strength and durability of mortar by hybrid GO/HO-G in comparison with the individual effects of GO or HO-G. In particular, when 0.015 wt% GO and 0.015 wt% HO-G were combined as multiple-additives added into cement mortar, the improvement ratio of compressive strength and chloride migration resistance at 28 days were 40.2% and 21.9%, which were far better than those of the mortar containing a single additive (0.03 wt% GO or 0.03 wt% HO-G). Additionally, the hybrid GO/HO-G not only could greatly reduce the degrada-tion of the fluidity of mortar as happened in the case of GO, but also further reinforced the flexural strength of cement composites when compared with its HO-G counterpart. The combination of these two nanofillers as multiple-nanoadditives for cement reinforcement is quite promising due to their synergistic effect and possesses strong potential for reinforcing and functionalizing cement composites.

Received 13th August 2022
Accepted 31st August 2022

DOI: 10.1039/d2ra05069b

rsc.li/rsc-advances

Open Access Article. Published on 21 September 2022. Downloaded on 3/10/2025 10:06:58 AM.
This article is licensed under a Creative Commons Attribution-NonCommercial 3.0 Unported Licence.

1 Introduction

Graphene-based nanosheets, a class of 2D materials that possess ultrahigh strength[1] have attracted lots of attention in the nano-reinforcement of cement composites recently.[2] However, the strong van der Waals forces and π–π stacking between the adjacent layers of graphene causes them to aggregate easily,[3,4] which creates challenges to achieve uniform dispersion in the hydrated cement slurry.[5] Besides, the weak interface force between the graphene nanosheets and the matrix also prevents their further applications.[6] As a derivative of graphene, GO also has excellent mechanical properties. Different from graphene, GO is an excellent hydrophilic material. The functional groups of GO not only facilitate its uniform dispersion in an aqueous solution but also provide an adequate interface interaction with the cement matrix.[7] Many studies have revealed that the mechanical durability of cement composites is enhanced significantly when blended with a very low content of GO.[8–10] Liu *et al.*[8] demonstrated that the increment of flexural strength of mortar was 21.86% when blended with 0.03% GO by cement mass. Therefore, GO has been widely used in nano-engineering cementitious materials. Hou *et al.*[11] studied the interface interaction between GO and calcium silicate hydrate (C–S–H) by molecular dynamics (MD) simulations, showing that the interface interaction of GO/C–S–H was stronger than that of graphene/C–S–H because the chemical bond connection was more stable. Zhang *et al.*[12] investigated the interfacial structure and energies of GO/C–S–H by MD method, confirmed that the chemical bond formed by the Ca^{2+} of C–S–H and the carboxyl groups on GO surface strengthened the interface adhesion of GO/C–S–H. Wang *et al.*[13] confirmed that a strong interaction between GO and cement matrix by the X-ray photoelectron spectroscope analyses (XPS) of the cement paste containing GO and a peak of $Ca(HCOO)_2$ at 347.4 eV was observed, which suggested the chemical reaction between Ca^{2+} and carboxyl group. As such, the strong interaction between GO and cement matrix was extremely essential for the enhancement of the cement composites by GO. However, the chemical cross-linking reaction with Ca^{2+} also hampered the homogeneous dispersion of GO in the cement matrix.[7]

[a]College of Materials Science and Engineering, Chongqing Jiaotong University, Chongqing 400074, China. E-mail: yuanxy@cqjtu.edu.cn

[b]School of Civil Engineering, Chongqing Jiaotong University, Chongqing 400074, China

† Electronic supplementary information (ESI) available. See https://doi.org/10.1039/d2ra05069b

© 2022 The Author(s). Published by the Royal Society of Chemistry

Open Access Article. Published on 21 September 2022. Downloaded on 3/10/2025 10:06:58 AM.
This article is licensed under a Creative Commons Attribution-NonCommercial 3.0 Unported Licence.

Several studies have reported that the carboxyl group on the GO sheet not only guarantees its excellent hydrophilicity but also enhances the interfacial strength of GO/C–S–H.[13,14] Even so, the negative impact of the carboxyl group on the dispersion of GO in the alkaline cement solution rich in Ca^{2+} cannot be ignored. The strong complexation ability of carboxylic groups with Ca^{2+} causes the adjacent GO sheets to cross-link each other and subsequently coagulate in the cement slurry.[15–17] The large GO deposits formed by agglomeration not only hinder the uniform dispersion of GO in the hydrated cement slurry but also harm the workability of cement composites,[7,10,18] thus the reinforcement effectiveness of cement composites by GO was severely limited.

In order to solve this problem, many scholars mixed other nanomaterials into cement matrix to study their reinforcement effect on cementitious materials.[19–26] Newell *et al.*[21] showed that significant improvements of the mechanical strength resulting from the combined addition of nanosilica (NS) and GO into the cement-based composites was achieved, and their reinforcement efficiency was obviously improved by increasing the superplasticizers dosage. Lu *et al.*[22] prepared GO-electrodeposited carbon fiber (CF) hybrid and found that compared with the CF reinforced cement paste, flexural strength of hybrid-fibers reinforced cement paste was enhanced by 10.53% when the GO/CF hybrid fibers were pre-dispersed in the GO solution and then mixed with cement powders. Li *et al.*[23] studied the effects of nanoalumina (NA) and GO on the early hydration and mechanical properties of Portland cement paste and showed that both NA and GO could efficiently accelerate cement hydration. As a physical filler, NA significantly accelerates the hydration of tricalcium aluminate (C_3A) in cement. On the other hand, compared to plain cement pastes, both the compressive and flexural strengths of cement pastes incorporating NA or GO are significantly increased. Yang *et al.*[24] investigated the reinforcement of GO/carbon nanotubes (CNTs) hybrid for cement paste and found a significant increase of the compressive strength (45.2%) when blended with 0.05% hybrid GO/CNTs by cement mass. Yuan *et al.*[25,26] evaluated the mechanical properties of cement mortar containing GO/graphene hybrid and found that the flexural and compressive strength of mortar enhanced significantly when blended with GO/G hybrid.

Similar to GO, hydroxylated-graphene (HO-G) also has excellent hydrophilicity which was achieved by introducing only hydroxyl groups onto the surface of graphene. Many people had reported the electrical and mechanical property of HO-G,[27–29] but its application in cement-based materials was rare. Yuan *et al.*[30] had thoroughly characterized the structure of HO-G prepared by ball-milling and confirmed that the fluidity of mortar containing HO-G was significantly better than that of the mortar blended with GO, that's because (i) the hydroxyl group is less hydrophilic than the carboxyl group and thus the free water in cement hydration medium absorbed on the surface of HO-G is less than that of GO. (ii) The HO-G ultimately effectively avoids the crosslinking reaction with aqueous Ca^{2+} leading to the efficient homogenous dispersion of 2D nanosheet in the hydrated cement slurry. However, the poor coordination ability of HO-G with Ca^{2+} also leads to weaker interfacial strength between HO-G and C–S–H. Theoretically, the advantages and disadvantages of HO-G as a nanofiller for cement composites are complementary to those of GO. As such, it is speculated that the hybrid HO-G/GO could exert their respective advantages and exhibit a strong synergistic reinforcing effect on the performance of cement composites when they are combined as multiple additives. Theoretically, HO-G was a 2D nanomaterial with a carbon benzene ring structure similar to GO, thus GO could be evenly dispersed in hydrated cement slurry with the assistance of HO-G. On the other hand, the hybrid HO-G/GO not only ensure good fluidity of fresh cement slurry but also provides sufficient interface interaction between nanosheets and matrix, thereby effectively exerting their reinforcing effect. Therefore, what might happen to the performance of cement composites when GO and HO-G were combined as multiple additives, which is also worthy of further study.

This paper aims to investigate the effect of hybrid GO/HO-G with various ratios on the macroscopic properties (workability, mechanical strength and durability) of cement composites when compared with that of individual GO and HO-G. Further, the microstructure and hydration degree of cement composite with the incorporation of hybrid GO/HO-G were evaluated by mercury intrusion porosimetry (MIP) and scanning electron microscopy (SEM), X-ray diffraction pattern (XRD) and non-evaporative water method (NEW), respectively. The results revealed that a synergistic enhancement effect of the hybrid GO/HO-G was exhibited on the performance of cement composites, which outperformed the reinforcement effect of individual GO or HO-G. This study provided a breakthrough in the reinforcement and functionalization of cement composites by combining GO and HO-G as multiple-additives for cement, and the hybrid GO/HO-G are excepted to further promote the application of graphene-based nanosheets in nano-engineering cement composites.

2 Experimental

2.1 Materials

The slurry of GO and the powder of graphite oxide were purchased from Sixth Element Materials Co., Ltd (Changzhou, China). HO-G was prepared by solid-state ball milling and its structure characterization was found in detail in Yuan's report.[30] The chemical composition and physical properties of Ordinary Portland cement type 42.5R cement (supplied by Yonggu New Building Material Co., Ltd) were shown in Tables S1 and S2.† The gradation of standard sand (purchased from Xiamen ISO Co., Ltd) was listed in Table S3.† Polycarboxylate superplasticizer (PCE) with a water-reducing rate and solid content of 26.7% and 50% was supplied by Kezhijie New Materials Co., Ltd. (Chongqing, China).

2.2 Preparation of cement mortars with different mass ratios of hybrid HO-G/GO

PCE was essential important in the practical application of concrete engineering, which was also confirmed to have an

© 2022 The Author(s). Published by the Royal Society of Chemistry

Open Access Article. Published on 21 September 2022. Downloaded on 3/10/2025 10:06:58 AM.
This article is licensed under a Creative Commons Attribution-NonCommercial 3.0 Unported Licence.

excellent ability to disperse GO in hydrated cement slurry.[31–33] Therefore, hybrid HO-G/GO solutions with different mass ratios were premixed with PCE, followed by mechanical ultrasound for 15 min using a 360 W ultrasonicator (UL transonic cleaner CH-06BM, Suzhou Chuanghui Electronics Co., Ltd.). After that, the nanosheets suspensions were added to the JJ-5 type cement mixer (Wuxi Jiangong Test Facility Co. Ltd., China) and mixed with the mixture of cement and sand. In this study, the amount of hybrid GO/HO-G was fixed as 0.03 wt% (the term "wt%" means the percentage by cement mass). The mixing procedure of mortar was conducted following Chinese National Standard GB/T 17671-1999. Different specimens based on the ratios of GO to HO-G were named as GxHy ($x = 1, 2, 3, 4, 5, 6, 7, 8, 9, y = 10 - x$), in which the ratio of x to y represented the mass ratio of GO to HO-G. The mortar specimen without GO and HO-G was denoted as the control group (PLAIN) and the mortar incorporated individually GO or HO-G with the dosage of 0.03 wt% was named as P_{GO} or $P_{HO\text{-}G}$. The mix compositions were listed in Table 1. After the stirring, the mortar mixture was cast in molds (40 × 40 × 160 mm) and compacted on a vibration table. Additionally, three Φ100 × 50 mm cylinders for each group were prepared for the test of rapid chloride migration (RCM). All the specimens were demoulded after 1 day and then cured in the standard curing room (20 °C/RH 90%) until the testing age.

2.3 Test method

Fourier transform infrared spectroscopy (FT-IR) was recorded on a Nicolet iS10 infrared spectrometer (Thermo electron corporation, UA). XPS analysis was carried out on a Thermo Fisher ESCALAB 250Xi photoelectron spectrometer (Waltham, MA, USA). A UV-3150 Spectrophotometer (Shimadzu Co., Ltd., Shanghai, China) was used to detect the maximum wavelength at the range of 200–800 nm.

The fluidity test of cement mortar was conducted following Chinese National Standard GB/T 2419-2005. The mechanical properties of compressive and flexural strength of the cement mortars were tested at the ages of 3, 7 and 28 days according to GB/T 17671-1999, the flexural strength was tested by three-point bending method. The anti chloride-ion penetration test shall be carried out in accordance with the RCM method in the Chinese Industry Standard JTG 3420-2020. MIP was tested according to National Standard GB/T 21650.1-2008 and performed with a MicroActive AutoPore V 9600 to test the porosity and pore size distribution of mortar specimens. The morphology of the specimens was evaluated by a Sigma300 scanning electron microscopy. XRD of powder mortar sample was recorded using a PANalytical X'Pert Pro powder diffract meter (PANalytical. Almelo, Netherlands).

2.4 Hydration degree

As a convenient and simple conventional method, the non-evaporative water (NEW) method was widely used to test the hydration degree of cementitious material.[34] The paste specimens were prepared by incorporation of hybrid GO/HO-G with various GO to HO-G ratios (1 : 9, 2 : 8, 3 : 7, 4 : 6, 5 : 5, 6 : 4, 7 : 3, 8 : 2 and 9 : 1). Again, the control group without nanosheets (PLAIN) and two groups containing GO and HO-G individuals (P_{GO} and $P_{HO\text{-}G}$) were also included. At the selected curing ages, the paste sample was ground after being soaked in ethyl alcohol for 24 h. Take out the sieved (80 μm) powder sample and subsequently pre-dried it in a vacuum oven at 65 °C until the weight remains constant. After that, the dried powder (approximately 1.5 g) was put into a Muffle furnace and heated to 1000 °C for 3 h. The NEW content was calculated according to eqn (1).[35]

$$m_w = [(100 - L)m_1 - 100m_2]/m_2 \quad (1)$$

where m_w is NEW content (%), L is the ignition loss of cement (1.25), m_1 is the weight of the sample before calcination (g), m_2 is the weight of the sample after high-temperature calcination (g).

3 Results and discussion

3.1 Characterization

From Fig. S1,† the typical AFM image displayed an irregular shape of GO sheet with the microscale lateral size of around 1 μm and the thickness of about 1.9 nm, corresponding to two or

Table 1 Mix proportions of different mortar groups

Samples	Cement (g)	Sand (g)	PCE[a] (%)	Water (g)	GO[a] (%)	HO-G[a] (%)	GO : HO-G[b]
PLAIN	450	1350	0.3	164.93	0	0	0
P_{GO}	450	1350	0.3	164.93	0.03	0	10 : 0
$P_{HO\text{-}G}$	450	1350	0.3	164.93	0	0.03	0 : 10
G_1H_9	450	1350	0.3	164.93	0.003	0.027	1 : 9
G_2H_8	450	1350	0.3	164.93	0.006	0.024	2 : 8
G_3H_7	450	1350	0.3	164.93	0.009	0.021	3 : 7
G_4H_6	450	1350	0.3	164.93	0.012	0.018	4 : 6
G_5H_5	450	1350	0.3	164.93	0.015	0.015	5 : 5
G_6H_4	450	1350	0.3	164.93	0.018	0.012	6 : 4
G_7H_3	450	1350	0.3	164.93	0.021	0.009	7 : 3
G_8H_2	450	1350	0.3	164.93	0.024	0.006	8 : 2
G_9H_1	450	1350	0.3	164.93	0.027	0.003	9 : 1

[a] Based on the weight percentage of cement weight. [b] The mass ratio of GO to HO-G.

Open Access Article. Published on 21 September 2022. Downloaded on 3/10/2025 10:06:58 AM.
This article is licensed under a Creative Commons Attribution-NonCommercial 3.0 Unported Licence.

three layers. The TEM image of GO sheet (Fig. S2†) presented an almost transparent flake with various wrinkles, and the lattice spacing of GO was 0.488 nm. UV-vis spectrum of HO-G, GO dispersions and nine groups of aqueous solutions of different GO : HO-G ratios (10 mg L^{-1}) were listed in Fig. S3.† An obvious peak at 230.4 nm and shoulder at 302.8 nm were illustrated in the result of GO, which attributed to the π–π* and n–π* transitions, respectively.[24,36] Different from the spectrum of GO, the result of HO-G displayed only a peak at 254.9 nm, corresponding to the sp^2 carbon structure of HO-G.[29] From Fig. S3,† with the increased proportion of HO-G, the maximum absorption peak wavelength of the hybrid solution exhibited red-shift, indicating that the π–π stacking was closely related to the ratio of GO to HO-G. Similar phenomenon was also found in other reports.[37,38]

Previous work confirmed that HO-G exhibits a more stable dispersion than GO in saturated $Ca(OH)_2$ solution often used to simulate the highly alkaline cement solution rich in Ca^{2+} (Fig. S4†), which could be explained by the poor coordination ability of HO-G with aqueous Ca^{2+} when compared to GO.[30] As such, the sediments of GO or HO-G formed by aggregation in the $CaCl_2$ solution (labeled as GO@Ca^{2+} or HO-G@Ca^{2+}) were characterized by FTIR, Raman and XPS to further investigate the chemical cross-linking between Ca^{2+} with GO or HO-G. From Fig. 1a, the FTIR spectrum of GO exhibited several characteristic peaks at 1051, 1223, 1613, 1726 and 3180 cm^{-1}, corresponding to the C–O, C–OH, C=C, C=O and the O–H, respectively.[13,39] While several peaks in the spectrum of GO@Ca^{2+} changed significantly compared to that of GO, including that the O–H stretching mode shifted from a wide and scattered peak to a sharp peak (3399 cm^{-1}), and the C=O tensile vibration peak of carboxyl group at 1726 cm^{-1} was significantly weakened, suggesting that the carboxyl group of GO was involved in the chemical reaction with Ca^{2+}.[13] The following functional group signals were observed in the spectrum of HO-G (Fig. 1b): the C–O groups (1386 and 1077 cm^{-1}), C=C groups (1631 cm^{-1}), C–H groups (2853 and 2982 cm^{-1}) and O–H stretching mode (3439 cm^{-1}).[29,30] While a new peak at 1455 cm^{-1} related to the bending vibration mode of calcium was detected in the spectrum of HO-G@Ca^{2+}, which corresponded to the Ca–O–C,[40] it could be explained as a weak chemical bonding formed by Ca^{2+} and the phenolic hydroxyl group at the edge of HO-G. Both Raman spectra of GO (Fig. 1c) and HO-G (Fig. 1d) showed three main peaks characteristic of the D-band (sp^3 carbon), G-band (sp^2 carbon) and 2D-band located at ~1350 cm^{-1}, ~1600 cm^{-1} and ~2700 cm^{-1}, respectively.[31] However, a clear blue shift of the D mode from 1349 to 1366 cm^{-1} and G mode from 1596 to 1598 cm^{-1} were observed in the Raman spectrum of GO@Ca^{2+} when compared to that of GO (Fig. 1c), suggesting that a strong chemical bonding between GO and Ca^{2+}.[41,42] Similarly, the D and G peaks in the spectrum of HO-G@Ca^{2+} also exhibited a slight blue shift compared to that of HO-G, indicating that there was a weak interaction between Ca^{2+} and HO-G.

XPS test was performed to investigate the nature of the functional groups of GO and HO-G. The XPS survey spectrum for GO (Fig. 2a) and HO-G (Fig. 2b) all displayed the presence of C 1s (283.97 eV) and O 1s (530.97 eV) core-levels. In addition to the peaks of C 1s and O 1s, the peaks of Ca 2p (*ca.* 346.97 eV) and Ca 2s (*ca.* 438.97 eV) were also detected in the XPS survey spectrum of GO@Ca^{2+} (Fig. 2a). At the same time, a faint peak at 345.97 eV related to Ca 2p was also detected in the survey spectrum of HO-G@Ca^{2+} (Fig. 2b), indicating that the interactions between HO-G and Ca^{2+} are weaker. From Fig. 2c, the high-resolution C 1s spectrum of GO displayed three function groups signal, including the C–C (*ca.* 284.77 eV), C–O (*ca.* 286.87

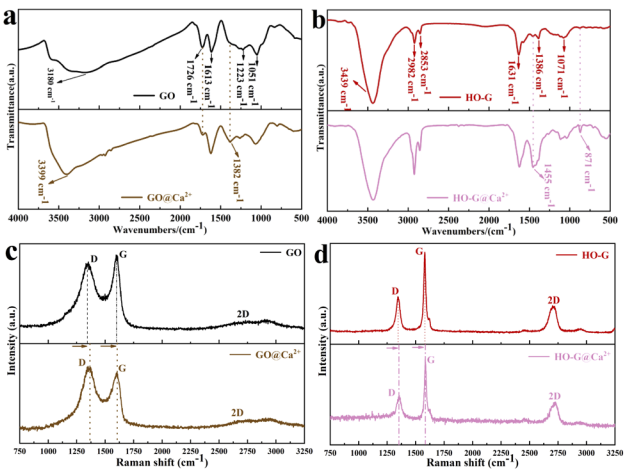

Fig. 1 FTIR spectra of (a) GO, GO@Ca^{2+} and (b) HO-G, HO-G@Ca^{2+}; Raman spectra of (c) GO, GO@Ca^{2+} and (d) HO-G, HO-G@Ca^{2+}.

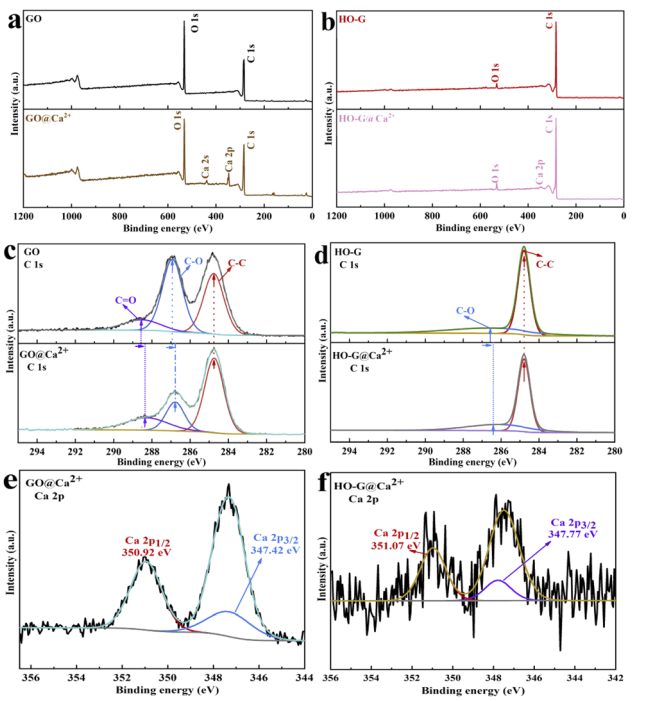

Fig. 2 XPS survey spectra of (a) GO, GO@Ca^{2+} and (b) HO-G, HO-G@Ca^{2+}; high-resolution XPS C 1s spectra of (c) GO, GO@Ca^{2+} and (d) HO-G, HO-G@Ca^{2+}; well-fitted XPS Ca 2p of (e) GO@Ca^{2+} and (f) HO-G@Ca^{2+}.

© 2022 The Author(s). Published by the Royal Society of Chemistry

Open Access Article. Published on 21 September 2022. Downloaded on 3/10/2025 10:06:58 AM.
This article is licensed under a Creative Commons Attribution-NonCommercial 3.0 Unported Licence.

eV) and C=O groups (*ca.* 288.62 eV), which was in line with other studies.[43,44] While a significant shift of the binding energies of C–O and C=O were observed in the C 1s spectrum of GO@Ca^{2+}(Fig. 2c), which further verified that there was chemical bonding between GO and Ca^{2+}. Besides, the well-fitted Ca 2p spectrum of GO@Ca^{2+} (Fig. 2e) exhibited the typical doublet of Ca $2p_{3/2}$ and Ca $2p_{1/2}$ at *ca.* 347.42 and *ca.* 350.92 eV corresponding to the $Ca(HCOO)_2$, suggesting that the reaction occurred between Ca^{2+} and carboxyl group of GO.[13,45] Fig. 2d presented the high-resolution C 1s spectrum of HO-G, only two peaks of C–C (*ca.* 284.62 eV) and C–O groups (*ca.* 286.22 eV) were observed, indicating that only the hydroxyl group existed in HO-G.[29,30] Worth noting that the binding energy of the C–O bond down-shifted slightly in the C 1s spectrum of HO-G@Ca^{2+} (Fig. 2d), which also confirmed that a new chemical vibration bond appeared in the HO-G@Ca^{2+} but the interactions between HO-G and Ca^{2+} were weaker. From Fig. 2f, two bands of Ca $2p_{3/2}$ at *ca.* 347.77 and Ca $2p_{1/2}$ at *ca.* 351.07 eV were observed which corresponded to the Ca–O bond, further indicating that reaction between Ca^{2+} and the phenolic hydroxyl group in HO-G.[46] According to the above discussion, it could be reasonably inferred that there was a certain chemical bond connection between HO-G and Ca^{2+}. However, the cross-linking reaction of Ca^{2+} with HO-G was considerably weaker than that of GO due to the poor coordination ability of phenolic hydroxyl groups with Ca^{2+}.

3.2 Workability of cement mortar containing HO-G/GO hybrid

The good fluidity of fresh cement slurry was a prerequisite to ensure workability and mechanical strength, which was very important for modern concrete engineering.[7,47] As shown in Fig. 3, the fluidity decreased when blended with nanomaterials in comparison with that of the PLAIN (213 mm). While P_{GO} showed the poorest fluidity of 177 mm, decreased by 16.9% relative to that of PLAIN. Similar results were reported in other reports.[7,48] The degradation of fluidity can be explained by two main reasons: (i) the large surface area and excellent hydrophilicity of GO could absorb the unbound water to its surfaces from hydrated cement slurry, thus resulting in a serious loss of fluidity[49] and this could be verified by the contact angle test (Fig. S5†). (ii) The cross-linking of adjacent GO sheets by Ca^{2+} through "bridging" the carboxyl groups of GO, leads to the formation of large sediment which hurts the workability of cement mortar seriously.[6,50] As for the sample incorporated of 0.03 wt% HO-G, only a slight loss of 1.9% in the fluidity (209 mm) was observed compared to that of the PLAIN. The reason could be that the free water in the cement hydration medium absorbed on the surface of HO-G was less than that of GO due to the hydroxyl group was less hydrophilic than carboxyl group, and the lack of active carboxyl groups within the structure of HO-G ultimately avoids the crosslinking reaction with aqueous Ca^{2+}, thus effectively avoids the aggregation of HO-G nanosheets in highly alkaline cement solution rich in calcium ion.[30] Due to the strong capability of hydrophilic GO to entrap free water from the hydrated cement slurry, the increasing proportion of GO in the hybrids showed a noticeable reduction in the fluidity of the cement slurry blended with HO-G/GO hybrid, which was observed from G_1H_9 to G_9H_1 samples.

3.3 Mechanical properties of cement mortar containing HO-G/GO hybrid

Many studies have confirmed that the optimal dosage of graphene-based materials for nanoengineered cement composites was 0.03 wt%.[8,30,35] As such, the total content of the hybrid was kept at 0.03 wt% for the convenience to compare the enhancement of different HO-G : GO ratios on the mechanic property of the mortar. Fig. 4 presented the compressive and flexural strength of different specimens at 3, 7 and 28 d, respectively. It can be observed that the incorporation of 0.03 wt% nanosheets in the mortar could significantly increase the compressive and flexural strength after different curing ages. As listed in Table S4,† compared with those of the PLAIN mortar, the compressive strengths (3, 7 and 28 d) of the mortar specimens containing pure GO and HO-G were increased by 23.3, 23.7, 17.1% and 32.1, 14.4, 15.6% at 3, 7 and 28 d, respectively. These results demonstrated that the compressive strength of mortar was improved significantly when blended

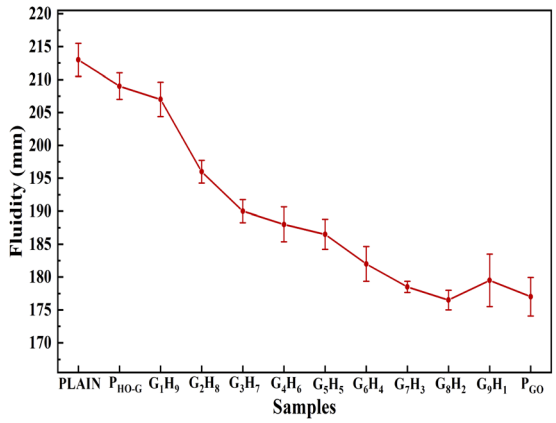

Fig. 3 The fluidity of different mortar groups.

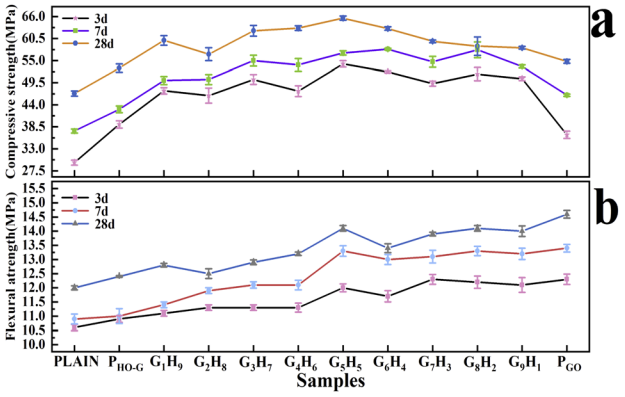

Fig. 4 The compressive (a) and flexural strength (b) of cement mortars with the hybrids of various GO : HO-G ratios.

Open Access Article. Published on 21 September 2022. Downloaded on 3/10/2025 10:06:58 AM. This article is licensed under a Creative Commons Attribution-NonCommercial 3.0 Unported Licence.

with a low amount of GO or HO-G. The reinforcement on the compressive strength of cement mortar could be ascribed to the well-known template effect and nano-filler effect of nanosheets.[7,51] More importantly, at the same dosage of nanofiller, higher compressive strengths were exhibited in all the nine hybrid groups compared to that of the mortar individually reinforced by GO or HO-G. From Table S5,† compared with the P_{HO-G}, the increasements of the compressive strength (28 d) of G_1H_9, G_2H_8, G_7H_3, G_6H_4, G_5H_5, G_6H_4, G_7H_3, G_8H_2 and G_9H_1 were 11.1, 4.6, 15.5, 16.6, 21.3, 16.5, 10.5, 8.3 and 7.6%, respectively. In addition, the compressive strength of G_1H_9, G_2H_8, G_7H_3, G_6H_4, G_5H_5, G_6H_4, G_7H_3, G_8H_2 and G_9H_1 at 28 d increased by 9.7, 3.3, 14.1, 15.1, 19.7, 15.0, 9.1, 6.9 and 6.2% in comparison with that of the P_{GO}, indicating that the dispersion of GO in the hydrated cement slurry was remarkably improved by HO-G, thus the enhancement effectiveness of GO was fully exerted. These results further highlight that there was a better synergistic effect of hybrid HO-G/GO for enhanced mechanic strength than the individual effects of GO or HO-G. The compressive strength of the mortar blended with HO-G/GO hybrid was promoted progressively with the increased proportion of GO in the hybrids from G_1H_9 to G_5H_5, followed by a decrease from G_5H_5 to G_9H_1. Notably, when the mass ratio of GO to HO-G was 5 : 5, G_5H_5 exhibited the largest improvement ratio on the compressive strength in comparison with PLAIN, the increments were 83.1, 51.7 and 40.2% at 3, 7 and 28 d, respectively.

Moreover, a significant improvement in the flexural strength of cement mortar could be observed with the addition of nanosheets (Fig. 4b). When GO was added to the mortar with the dosage of 0.03 wt%, it provided an additional 16.0, 22.9, 21.7% enhancements of flexural strength in contrast with that of the PLAIN at 3, 7 and 28 days, demonstrating that GO could significantly improve the flexural strength of mortar, which was consistent with previous reports.[33,52] While the incorporation of 0.03 wt% HO-G only gave 2.8, 1.8 and 3.3% increments in flexural strength of mortar after curing for 3, 7, 28 d, respectively. In addition, the flexural strength (28 d) of G_1H_9, G_2H_8, G_7H_3, G_6H_4, G_5H_5, G_6H_4, G_7H_3, G_8H_2 and G_9H_1 were increased by 3.3, 6.7, 4.2, 7.5, 10.0, 17.5, 11.7, 15.8, 17.5 and 16.7% when compared with that of the PLAIN (Table S4†). It could be reasonably explained as follows: the formation of chemical bonds between carboxyl groups and Ca^{2+} afforded a strong interface interaction of GO/C–S–H,[30,53,54] which could transfer the applied load to the nano-reinforcer at the interface and prevent the extension of micro-cracks.[19] But the poor coordination ability of phenolic hydroxyl group with Ca^{2+} leads to an intrinsically weak strength between HO-G and cement matrix. Therefore, a noticeable improvement in the flexural strength of the mortar incorporated by HO-G/GO hybrid could be observed with the increasing proportion of GO in the hybrids from G_1H_9 to G_9H_1. As listed in Table S6,† the increments of G_1H_9, G_2H_8, G_7H_3, G_6H_4, G_5H_5, G_6H_4, G_7H_3, G_8H_2 and G_9H_1 on the flexural strength were 3.2, 0.8, 4.0, 6.5, 13.7, 8.1, 12.1, 13.7 and 12.9% when compared with that of P_{HO-G}, which highlighted that the important role of GO in the improved interface strength for the cement composites. According to the above results, the complementary effect between GO and HO-G was further confirmed: (i) GO could be evenly dispersed in hydrated cement matrix with the assistance of HO-G, thus the reinforcing effect of GO was fully exerted. (ii) At the same time, the uniformly dispersed GO could further compensate for the weak interface between HO-G and the cement matrix. As such, the hybrid HO-G/GO could exert their respective advantages and exhibit a strong synergistic reinforcing effect on the performance of cement composites when they are combined as multiple additives.

Combined with the results of fluidity and compressive strength, G_5H_5 also exhibited remarkable increments of 13.2, 22.0, 17.5% in the flexural strength compared to that of PLAIN at the curing age of 3, 7 and 28 d. As such, it could be inferred that the optimal ratio of GO to HO-G was 5 : 5. Additionally, compared with the reinforcing enhancements by other nanomaterials collected in Table 2, the enhancement of hybrid HO-G/GO on the mechanical properties of cement composite was more significant. Especially, the incorporation of a very low amount of hybrids not only shows a great reinforcement but also was cost-effective. As such, the hybrid HO-G/GO holds the strong potential to promote the application of graphene-based nanosheets in nano-engineering cement composites.

3.4 Chloride-ion penetration resistance of cement mortar

The long-term performance of concrete is severely affected by several chemical corrosion (*e.g.* Cl^- and SO_4^{2-}), so it's necessary to study the durability of concrete.[7,60] The non-steady-state migration coefficient (D_{RCM}) for each group was measured to evaluate the durability of mortar containing hybrid GO/HO-G in this study. Table 3 presented the results of chloride penetration depth (X_d) and D_{RCM} for all mortar specimens at 28 days. Upon the incorporation of 0.03 wt% GO into the cement mortar, a significant reduction was observed in X_d and D_{RCM} by 16.9% and 16.4% in comparison with that of PLAIN, indicating that the ingress of chloride was reduced significantly in the mortar when blended with a low amount of GO, which was consistent with other reports.[60] Similarly, the X_d and D_{RCM} of the mortar containing 0.03 wt% HO-G degraded by 14.5% and 13.7% compared to that of the plain specimen, suggesting that HO-G also contributes to effectively interdict the transport channels of Cl^- and thus enhance the resistance of cement matrix against chloride invasion as what happened in the case of GO.[30,61] The improved resistance against chloride penetration could be attributed to the nano-filler effect of nanosheets which contributes to forming a compact structure and strong barriers within the cement matrix.[2] Worth noting that the samples containing various ratios of hybrid GO/HO-G (the total dosage was fixed at 0.03 wt%) exhibited much lower X_d and D_{RCM} in contrast with the specimens individually incorporated of GO or HO-G, highlighting the co-effect of GO and HO-G on the chloride migration resistance of cement mortars and further confirmed that GO could be evenly dispersed in the cement matrix with the assistance of HO-G. Notably, when the ratio of GO to HO-G was 5 : 5, the specimen (G_5H_5) exhibited maximum performance from the reduction of X_d and D_{RCM} by 22.0% and

 © 2022 The Author(s). Published by the Royal Society of Chemistry

Open Access Article. Published on 21 September 2022. Downloaded on 3/10/2025 10:06:58 AM.
This article is licensed under a Creative Commons Attribution-NonCommercial 3.0 Unported Licence.

Table 2 The enhancement of nanofillers on the mechanical properties of cement composites

Nanofillers	Optimal dosage[a] (wt%)	Enhancement of the mechanical properties in 28 d (%)		References
		Compressive strength	Flexural strength	
Nano silica (nano-SiO_2)	2	10.1	11.0	Shi *et al.*[55]
Nano-alumina (nano-Al_2O_3)	1	18.46	6.27	Ge *et al.*[56]
Nano-calcium carbonate (nano-$CaCO_3$)	2	3.23	4.68	Cosentino *et al.*[57]
Nano-titanium oxide (nano-TiO_2)	0.75	19.33	15.1	Salman *et al.*[58]
Carbon nanotubes (CNTs)	0.05	6.4	10.1	Du *et al.*[59]
Graphene oxide (GO)	0.03	5.16	21.86	Liu *et al.*[8]
Hydroxylated-graphene (HO-G)	0.03	21.19	7.89	Yuan *et al.*[30]
Hybrid GO/HO-G	0.03[b]	40.2	17.5	This study

[a] Based on the weight percentage of cement weight. [b] The mass ratio of GO to HO-G was 5 : 5 (0.015 wt% GO + 0.015 wt% HO-G).

21.9% compared to the PLAIN specimen, which further confirmed that the best proportion of GO to HO-G was 5 : 5. As discussed above, the combination of GO and HO-G is expected to exhibit more positive synergistic effect on improving the durability of cement composites than the individual GO and HO-G.

3.5 Morphology and pore structure of cement mortars

Well-known is that the microstructure of hardened cement slurry is complex which contains many micro-cracks and holes, and the macroscopic properties of cement composites are closely associated with the pore structure.[62,63] As such, it's helpful to evaluate the influence of GO and HO-G on the microstructure of the cement composites by investigating the pore structure. The pore size distribution and porosity for PLAIN, P_{GO}, $P_{HO\text{-}G}$ and G_5H_5 were tested by MIP after curing for 28 days. It can be observed that multi-peaks in the differential mercury curves (Fig. 5a) of all the samples, indicating that there are pores of different sizes in the hardened cement mortars. According to the literature,[64,65] the pores in cement composites can be divided into gel pores (2.5–10 nm), transition pores (10–100 nm), capillary pores (100–1000 nm) and macropores (exceeding 1000 nm). It is widely accepted that the transport and mechanical properties of cement composites are affected more by macropores which also were defined as harmful pores.[66] As shown in Fig. 5a, a single peak at a pore diameter from 40–50 nm was exhibited in all the curves for the PLAIN, P_{GO}, $P_{HO\text{-}G}$ and G_5H_5 mortar, which corresponded to the critical pore size.[49,61] With the incorporation of HO-G or hybrid GO/HO-G, the volume of the critical pore decreased significantly, indicating that the pore structure of cement composites was refined by HO-G or hybrid GO/HO-G. In addition, it also can be observed that the macropores of the mortar containing nanosheets degrade significantly in comparison with the PLAIN sample, suggesting that the addition of nanosheets could result in fewer macropores of the mortar. When added nanosheets to the mortar, an increase in the portion of capillary pore was observed, which could be ascribed to the layer-like structure of nanosheets.[60] Bykkam *et al.*[67] reported that some sheets of nanomaterial connected each other and formed a multi-void structure, which lead to the increase of capillary pores in the mortar. The cumulative pore volume curves were shown in Fig. 5b, compared to the PLAIN specimen, the curves of P_{GO}, $P_{HO\text{-}G}$ and G_5H_5 downward-shift demonstrated the refinement of pore structure in the mortar. Besides, the total porosity of the mortar incorporation of GO (10.89%), HO-G (10.63%) were degraded by 0.73%, 3.1% in comparison to that of the plain

Table 3 Chloride penetration depth and non-steady-state migration coefficient for different mortar groups

Samples	X_m[a] (mm)	X_d[b] (mm)/change[c] (%)	D_{RCM} ($\times 10^{-12}$ m^2 s^{-1})/change[c] (%)
PLAIN	50.3	25.5/0	14.6/0
P_{GO}	50.5	21.2/−16.9	12.2/−16.4
$P_{HO\text{-}G}$	50.3	21.8/−14.5	12.6/−13.7
G_1H_9	50.2	21.5/−15.7	12.2/−16.4
G_2H_8	50.0	20.8/−18.4	11.9/−18.5
G_3H_7	50.2	20.9/−18.0	11.9/−18.5
G_4H_6	50.5	20.5/−19.61	11.8/−19.2
G_5H_5	50.3	19.9/−22.0	11.4/−21.9
G_6H_4	50.4	20.2/−20.8	11.7/−19.9
G_7H_3	50.0	20.4/−20.0	11.9/−18.5
G_8H_2	50.5	20.4/−20.0	11.7/−19.9
G_9H_1	50.7	21/−17.7	12.0/−17.8

[a] X_m represents the height of specimens. [b] X_d represents chloride penetration depth. [c] Compared to the PLAIN.

Open Access Article. Published on 21 September 2022. Downloaded on 3/10/2025 10:06:58 AM.
This article is licensed under a Creative Commons Attribution-NonCommercial 3.0 Unported Licence.

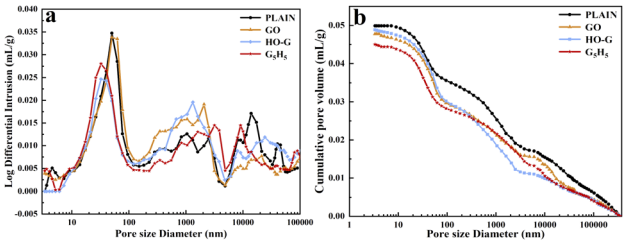

Fig. 5 (a) Pore size distribution curves and (b) cumulative pore volume curves of the PLAIN, P_{GO}, P_{HO-G} and G_5H_5.

sample (10.97%), which could be attributed to the nano-filler effect of nanosheets.[68] The more noticeable reduction (8.11%) in the porosity of G_5H_5 than that of the specimens containing GO and HO-G individuals highlighted a better synergistic effect of hybrid GO/HO-G, which further verified that the dispersion of GO in the cement matrix was improved by HO-G, thus the nano-filling effect of GO could be fully exerted. As such, superior performance could be further achieved by combining these two nanomaterials.

Fig. 6 displayed the SEM images of the fracture section of PLAIN, P_{HO-G}, P_{GO} and G_5H_5 at 28 days. The PLAIN specimen presented an irregular and non-compact morphology with various microcracks and holes (Fig. 6a), the hydration crystals were mostly amorphous and the growth was irregular and disorderly, thus producing plenty of interfacial gaps (Fig. 6b). The SEM images of P_{HO-G} (Fig. 6c and d) presented a compact morphology without obvious large holes and cracks, which attributed to the nano-filler effect of graphene. From Fig. 6e and f, the images of P_{GO} displayed a regular polyhedral structure, this could be attributed to the active functional groups in the surface of GO provided the growth points of the hydration crystals and could be able to link the hydration products in the cement hydration medium, thus exhibited the seeding effects and template effects to favor the ordered growth of crystals.[69–71] The micro-morphology of the G_5H_5 was shown in Fig. 6g and h, it is of note that the hydration crystals are now organized into networks of flower-like patterns which fill in the interfacial gaps. From Fig. 6g, a more regular and compact structure was observed than that of P_{HO-G} and P_{GO}. A clear cluster of flower-like crystals can be observed from the magnified SEM image (Fig. 6h), and the hydration crystals form a regular structure by crosslinking and interweaving, indicating that GO could be more evenly dispersed in cement matrix with the assistance of HO-G to provide more growth points. At the same time, the growth patterns of the hydration crystals were induced by the seeding effect and template effects of GO/HO-G, and thus a fully bloomed flower-like crystal could be formed by some neighboring hydration products (*e.g.* AFt, AFm, $Ca(OH)_2$).[71,72] According to the above results, it could be further inferred that the action principle of hybrid GO/HO-G: on the one hand, the dispersion of GO in the hydrated cement slurry was remarkably improved by HO-G, thus the seeding effect of GO was fully exerted and further improved the microstructure. On the other hand, the uniformly dispersed GO could further compensate for the weak interface between HO-G and the cement matrix. As such, the hybrid HO-G/GO could exert their respective advantages and exhibit a strong synergistic reinforcing effect on the performance of cement composites when they are combined as multiple additives.

XRD patterns of different hardened mortar specimens at the curing age of 28 d are shown in Fig. 7. It can be seen that the

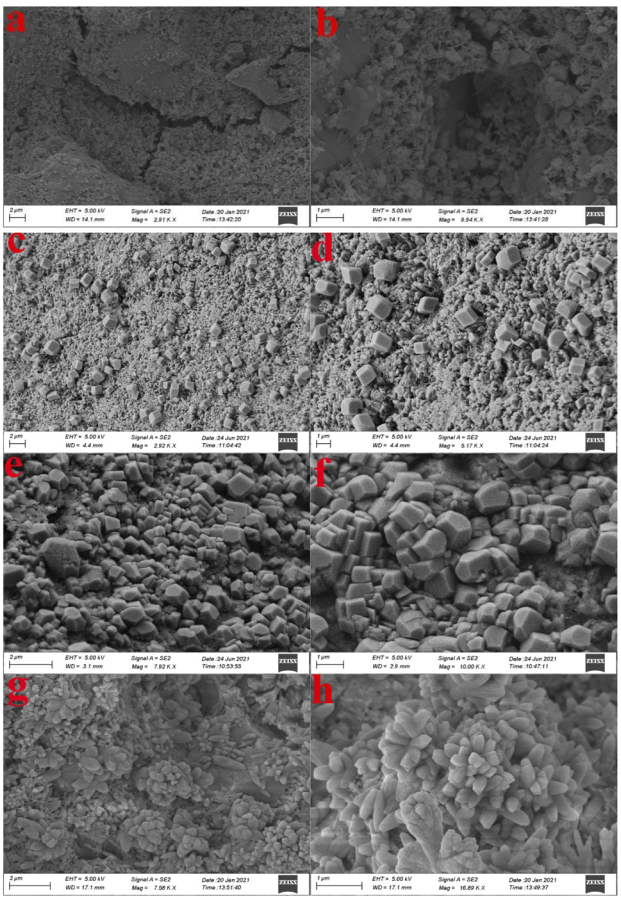

Fig. 6 SEM images of the PLAIN (a, b) P_{HO-G} (c, d), P_{GO} (e, f) and G_5H_5 (g, h) cured at 28 days.

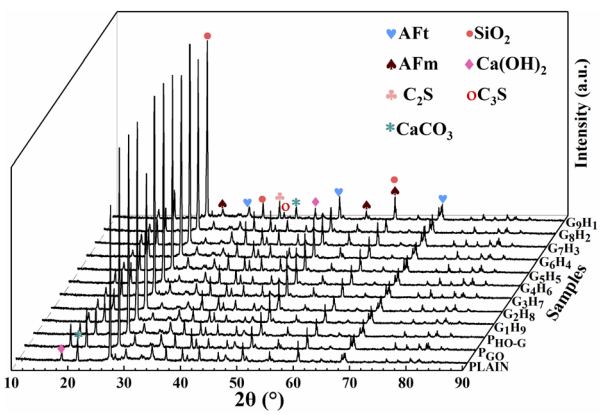

Fig. 7 XRD patterns of the different mortar specimens after curing for 28 days.

© 2022 The Author(s). Published by the Royal Society of Chemistry

Open Access Article. Published on 21 September 2022. Downloaded on 3/10/2025 10:06:58 AM.
This article is licensed under a Creative Commons Attribution-NonCommercial 3.0 Unported Licence.

XRD spectrums of PLAIN, P_{GO}, $P_{HO\text{-}G}$, G_1H_9, G_2H_8, G_7H_3, G_6H_4, G_5H_5, G_6H_4, G_7H_3, G_8H_2 and G_9H_1 all have similar peaks profile, indicating that the addition of nanosheets didn't affect the structure and type of hydrated crystals in the cement mortar.[69] Several crystals of cement hydration products were discerned in these XRD spectra, which included portlandite (CH) at 18.2° and 46.0°, monosulfates (AFm) at 29.5°, 55.0°, 60.1°, Silicon dioxide (SiO_2) at 26.8°, 36.7°, calcarea carbonica ($CaCO_3$) at 21.2°, 42.6°, tricalcium silicate (C_3S) at 40.4°, dicalcium silicate (C_2S) at 39.6°, and ettringite (AFt) at positions of 34.2°, 50.3° and 68.4°, respectively.[69,73,74] Compared to the results of the PLAIN, although the diffraction peaks profiles were similar, the intensity of some crystal peaks have changed when added nanosheets to the mortar. From Fig. 7, when the mortar was incorporated with 0.03 wt% HO-G and GO individuals, the diffraction peak intensity of CH (18.2°) and AFt (50.3°) increased in comparison with that of PLAIN, suggesting that the accelerated cement hydration generated more hydration products at the presence of GO and HO-G, highlighting that the seeding effects of graphene.[9,48] Worth noting that the diffraction peak intensity of AFt (50.3°) increased more obviously when incorporated with hybrid GO/HO-G, indicating that the combination of these two materials could further accelerate cement hydration. Generally, AFt negatively affected the mechanical strength of cement composite, especially for the flexural strength. In this study, the XRD results indicated that the diffraction peak intensity of AFt (50.3°) increased more obviously when incorporated with hybrid GO/HO-G, but from Fig. 4b, the results showed that a significant improvement in the flexural strength of cement mortar could be observed with the addition of hybrid GO/HO-G. Lv *et al.*[71] found that the flower-like crystals benefit enhanced toughness because the flower-like crystals consisted of interwoven rodlike crystals and there was a certain space to absorb movement and thus the tensile and flexural strengths were greater. The flower-like hydration crystals were observed in GO/HO-G hybrid blended cement system and AFt didn't obviously weaken the flexural strength of the resulting composite despite that its content was more than that of the plain sample as seen from the increased diffraction peak intensity of AFt (50.3°) in the XRD pattern. As such, the formation of much more regular flower-like crystals (Fig. 6g and h) indicated that the process of cement hydration was accelerated and the growth of hydrated crystals was regularized by the synergistic effect of hybrids, thereby improving the microstructure of cement mortar.

3.6 Hydration degree

In this work, the NEW content of cement pastes at 1, 3 and 28 d were tested to study the effect of nanosheets on the hydration degree of the cement. Fig. 8 presented the histograms of NEW content of PLAIN, P_{GO}, $P_{HO\text{-}G}$, G_1H_9, G_2H_8, G_7H_3, G_6H_4, G_5H_5, G_6H_4, G_7H_3, G_8H_2 and G_9H_1 at different ages, it can be seen that the NEW content of all the specimens increased as the extension of curing age. The NEW content of the samples (P_{GO}, $P_{HO\text{-}G}$, G_1H_9, G_2H_8, G_7H_3, G_6H_4, G_5H_5, G_6H_4, G_7H_3, G_8H_2 and G_9H_1) increased when compared to that of the PLAIN after curing for 1 day. The NEW content of P_{GO} and $P_{HO\text{-}G}$ increased by 1.9% and

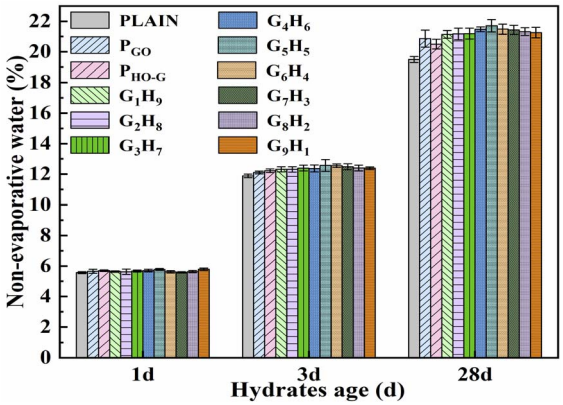

Fig. 8 NEW content of different paste specimens at different curing ages.

2.8% in comparison with that of PLAIN at the age of 3 days. In addition, the NEW content of the specimens incorporated of hybrid GO/HO-G were further increased in comparison with that of the specimens individually incorporated with GO or HO-G. Notably, the G_5H_5 showed a 5.8% increment in the NEW content, relative to the PLAIN. Combined with the results of 1 and 3 days, it can be reasonably inferred that the early hydration degree of cement was accelerated by a low dosage of nanosheets so that more hydrated crystals were generated.[35,75] Especially, a more significant effect on the early hydration of the cement system can be performed by the incorporation of hybrid GO/HO-G. The NEW content of P_{GO} and $P_{HO\text{-}G}$ increased by 7.0% and 5.2% compared with that of PALIN at the curing age of 28 d, indicating that the effect of GO on promoting the hydration of the later stage for the cement system was more obvious than that of HO-G. Besides, the increment of the NEW content for G_1H_9, G_2H_8, G_7H_3, G_6H_4, G_5H_5, G_6H_4, G_7H_3, G_8H_2 and G_9H_1 were 8.4, 8.6, 8.7, 10.1, 11.3, 10.2, 9.9, 9.3 and 9.0%, respectively. All the hybrids groups exhibited more obvious increments of the NEW content when compared with that of P_{GO} and $P_{HO\text{-}G}$, further highlighting the co-effect of these two nanofillers on the accelerated cement hydration.

4 Conclusion

This study investigated the co-effect of hybrid graphene oxide (GO)/hydroxylated-graphene (HO-G) with various ratios on the macro-properties and microstructure of cement composites. Compared with GO or HO-G individuals, the hybrid GO/HO-G could make full use of their respective merits and their synergistic effect on the improved performance of the resulting cement composites was very remarkable when they were combined as multiple additives added into cement composites. On the one hand, the hybrid GO/HO-G could greatly reduce the loss of fluidity of mortar as terribly happened in the case of GO, so that the workability of cement composites wasn't frustrating when applied in cement engineering. On the other hand, the hybrid GO/HO-G could effectively generate the interfacial interaction with cement matrix when compared with the HO-G

Open Access Article. Published on 21 September 2022. Downloaded on 3/10/2025 10:06:58 AM. This article is licensed under a Creative Commons Attribution-NonCommercial 3.0 Unported Licence.

individuals, thus further enhancing the mechanical strength of cement composites. In contrast, the hybrid GO/HO-G exhibited a synergistic improvement in the mechanical and durability of the cement mortars outnumbering the individual effects of GO and HO-G, especially when the ratio of GO to HO-G is 5 : 5. In addition, when GO and HO-G were combined as multiple additives, the hybrids exhibited a better synergistic effect on the refinement of pore structure, accelerated the hydration degree and regulated the growth of hydration crystals. In conclusion, the hybrid GO/HO-G are expected to exhibit a great application prospect for nano-engineering cement composites.

Conflicts of interest

There are no conflicts of interest to declare.

Acknowledgements

The authors would like to gratefully acknowledge the financial supports from the National Natural Science Foundation of China (51402030), Natural Science Foundation of the Chongqing Science and Technology Commission (cstc2017jcyjBX0028), Science and Technology Research Program of Chongqing Municipal Education Commission (KJZD-K201800703).

Notes and references

1 V. B. Mohan, K.-t. Lau, D. Hui and D. Bhattacharyya, *Composites, Part B*, 2018, **142**, 200–220.
2 Y. Lin and H. Du, *Constr. Build. Mater.*, 2020, **265**, 120312–120327.
3 A. D. Ghuge, A. R. Shirode and V. J. Kadam, *Curr. Drug Targets*, 2017, **18**, 724–733.
4 H. Du and S. D. Pang, *Constr. Build. Mater.*, 2018, **167**, 403–413.
5 H. Yang, H. Cui, W. Tang, Z. Li, N. Han and F. Xing, *Composites, Part A*, 2017, **102**, 273–296.
6 M. F. Kai, L. W. Zhang and K. M. Liew, *Carbon*, 2019, **146**, 181–193.
7 L. Zhao, X. Guo, L. Song, Y. Song, G. Dai and J. Liu, *Constr. Build. Mater.*, 2020, **241**, 117939–117955.
8 H. Peng, Y. Ge, C. S. Cai, Y. Zhang and Z. Liu, *Constr. Build. Mater.*, 2019, **194**, 102–109.
9 J. Liu, J. Fu, Y. Yang and C. Gu, *Constr. Build. Mater.*, 2019, **199**, 1–11.
10 Y. Xu, J. Zeng, W. Chen, R. Jin, B. Li and Z. Pan, *Constr. Build. Mater.*, 2018, **171**, 291–302.
11 P. Wang, G. Qiao, Y. Guo, Y. Zhang, D. Hou, Z. Jin, J. Zhang, M. Wang and X. Hu, *Constr. Build. Mater.*, 2020, **260**, 119927–119936.
12 H. Wan and Y. Zhang, *Mater. Struct.*, 2020, **53**, 34–45.
13 M. Wang, R. Wang, H. Yao, S. Farhan, S. Zheng and C. Du, *Constr. Build. Mater.*, 2016, **126**, 730–739.
14 S. Sharma and N. C. Kothiyal, *RSC Adv.*, 2015, **5**, 52642–52657.
15 K. Yang, B. Chen, X. Zhu and B. Xing, *Environ. Sci. Technol.*, 2016, **50**, 11066–11075.
16 L. Wu, L. Liu, B. Gao, R. Muñoz-Carpena, M. Zhang, H. Chen, Z. Zhou and H. J. L. Wang, *Langmuir*, 2013, **29**, 15174–15181.
17 Y. Jiang, R. Raliya, P. Liao, P. Biswas and J. D. Fortner, *Environ. Sci.: Nano*, 2017, **4**, 1484–1493.
18 S. Ghazizadeh, P. Duffour, N. T. Skipper, M. Billing and Y. Bai, *Cem. Concr. Res.*, 2017, **99**, 116–128.
19 Z. Lu, D. Hou, L. Meng, G. Sun, C. Lu and Z. Li, *RSC Adv.*, 2015, **5**, 100598–100605.
20 Y. Du, J. Yang, B. Skariah Thomas, L. Li, H. Li, W. Mohamed Shaban and W. Tung Chong, *Constr. Build. Mater.*, 2020, **260**, 120449–120459.
21 M. Newell and E. Garcia-Taengua, *Constr. Build. Mater.*, 2019, **221**, 433–442.
22 Z. Lu, A. Hanif, G. Sun, R. Liang, P. Parthasarathy and Z. Li, *Cem. Concr. Compos.*, 2018, **87**, 220–228.
23 W. Li, X. Li, S. J. Chen, G. Long, Y. M. Liu and W. H. Duan, *J. Mater. Civ. Eng.*, 2017, **29**, 04017087–04017095.
24 Y. Du, J. Yang, B. Skariah Thomas, L. Li, H. Li and S. Nazar, *Constr. Build. Mater.*, 2020, **261**, 119815–119824.
25 L. Yang and X. Yuan, *J. Funct. Mater*, 2019, **50**, 12089–12096.
26 X. Yuan, J. Zeng, J. Gao and G. Xiao, *J. Chongqing Jiaotong Univ.*, 2019, **38**, 45–50.
27 C. Qin, H. Deng, S. Ao, Z. Dai, J. Huang, H. Ni and P. Ye, *Carbon*, 2021, **176**, 290–295.
28 J. H. Ding, O. U. Rahman, H. R. Zhao, W. J. Peng, H. M. Dou, H. Chen and H. B. Yu, *Nanotechnology*, 2017, **28**, 39LT01–39LT20.
29 J. Sun, Y. Deng, J. P. Li, G. Wang, P. He, S. Y. Tian, X. M. Bu, Z. F. Di, S. W. Yang, G. Q. Ding and X. M. Xie, *ACS Appl. Mater. Interfaces*, 2016, **8**, 10226–10233.
30 S. Yang, W. Jia, Y. Wang, W. Zhang and X. Yuan, *ACS Omega*, 2021, **6**, 30465–30477.
31 Z. Lu, A. Hanif, C. Ning, H. Shao, R. Yin and Z. Li, *Mater. Des.*, 2017, **127**, 154–161.
32 Q. Wang, S.-y. Li, S. Pan and Z.-w. Guo, *New Carbon Mater.*, 2018, **33**, 131–139.
33 L. Zhao, X. Guo, C. Ge, Q. Li, L. Guo, X. Shu and J. Liu, *Composites, Part B*, 2017, **113**, 308–316.
34 X.-M. Kong, H. Liu, Z.-B. Lu and D.-M. Wang, *Cem. Concr. Res.*, 2015, **67**, 168–178.
35 Z. Wei, Y. Wang, M. Qi, J. Bi, S. Yang and X. Yuan, *Constr. Build. Mater.*, 2021, **293**, 123507–123516.
36 X. Li, A. H. Korayem, C. Li, Y. Liu, H. He, J. G. Sanjayan and W. H. Duan, *Constr. Build. Mater.*, 2016, **123**, 327–335.
37 H. Gao, G. Hu and H. Liu, *Ind. Eng. Chem. Res.*, 2019, **58**, 17842–17849.
38 C. Zhang, L. L. Ren, X. Y. Wang and T. X. Liu, *J. Phys. Chem. C*, 2010, **114**, 11435–11440.
39 A. Alkhouzaam, H. Qiblawey, M. Khraisheh, M. Atieh and M. Al-Ghouti, *Ceram. Int.*, 2020, **46**, 23997–24007.
40 A. Rastinfard, M. H. Nazarpak and F. Moztarzadeh, *RSC Adv.*, 2018, **8**, 91–101.
41 X. Yuan, J. Niu, J. Zeng and Q. Jing, *Nanomaterials*, 2018, **8**, 574–587.
42 T. Tong, Z. Fan, Q. Liu, S. Wang, S. Tan and Q. Yu, *Constr. Build. Mater.*, 2016, **106**, 102–114.

© 2022 The Author(s). Published by the Royal Society of Chemistry

Open Access Article. Published on 21 September 2022. Downloaded on 3/10/2025 10:06:58 AM.
This article is licensed under a Creative Commons Attribution-NonCommercial 3.0 Unported Licence.

43 R. Al-Gaashani, A. Najjar, Y. Zakaria, S. Mansour and M. A. Atieh, *Ceram. Int.*, 2019, **45**, 14439–14448.
44 R. Muzyka, S. Drewniak, T. Pustelny, M. Sajdak and L. Drewniak, *Materials*, 2021, **14**, 769–782.
45 L. Zhao, X. Guo, Y. Liu, Y. Zhao, Z. Chen, Y. Zhang, L. Guo, X. Shu and J. Liu, *Constr. Build. Mater.*, 2018, **190**, 150–163.
46 S. Zhang, Z. Lin, G. Jiang, J. Wang and D.-Y. Wang, *Compos. Sci. Technol.*, 2018, **159**, 59–69.
47 M. Wang, H. Yao, R. Wang and S. Zheng, *Constr. Build. Mater.*, 2017, **150**, 150–156.
48 M. Birenboim, R. Nadiv, A. Alatawna, M. Buzaglo, G. Schahar, J. Lee, G. Kim, A. Peled and O. Regev, *Composites, Part B*, 2019, **161**, 68–76.
49 X. Li, Y. M. Liu, W. G. Li, C. Y. Li, J. G. Sanjayan, W. H. Duan and Z. Li, *Constr. Build. Mater.*, 2017, **145**, 402–410.
50 L. Zhao, X. Guo, Y. Liu, C. Ge, Z. Chen, L. Guo, X. Shu and J. Liu, *Carbon*, 2018, **127**, 255–269.
51 Z. Zhao, T. Qi, W. Zhou, D. Hui, C. Xiao, J. Qi, Z. Zheng and Z. Zhao, *Nanotechnol. Rev.*, 2020, **9**, 303–322.
52 S. H. Lv, H. Y. Hu, J. Zhang, Y. Lei, L. Sun and Y. G. Hou, *Struct. Concr.*, 2019, **20**, 471–482.
53 D. Hou, T. Yang, J. Tang and S. Li, *Phys. Chem. Chem. Phys.*, 2018, **20**, 8773–8789.
54 R. Kaur and N. C. Kothiyal, *Constr. Build. Mater.*, 2019, **222**, 358–370.
55 Y. Cheng and Z. Shi, *Adv. Civ. Eng.*, 2019, **2019**, 1–9.
56 A. Zhang, W. Yang, Y. Ge, Y. Du and P. Liu, *J. Build. Eng.*, 2021, **34**, 101936–101947.
57 I. Cosentino, F. Liendo, M. Arduino, L. Restuccia and G. A. Ferro, *Procedia Struct. Integr*, 2020, **26**, 155–165.
58 M. M. Salman, K. M. Eweed and A. M. Hameed, *Al-Nahrain J. Eng. Sci.*, 2017, **19**, 265–270.
59 M. R. Du, H. W. Jing, Y. Gao, H. J. Su and H. Y. Fang, *Nanotechnol. Rev.*, 2020, **9**, 115–135.
60 A. Mohammed, J. G. Sanjayan, W. H. Duan and A. Nazari, *Constr. Build. Mater.*, 2015, **84**, 341–347.
61 H. Du and S. D. Pang, *Cem. Concr. Res.*, 2015, **76**, 10–19.
62 G. Bastos, F. Patino-Barbeito, F. Patino-Cambeiro and J. Armesto, *Materials*, 2016, **9**, 1015–1044.
63 M. Sun, C. Zou and D. Xin, *Cem. Concr. Compos.*, 2020, **114**, 103731–103748.
64 Q. Wang, J. Wang, C.-x. Lu, B.-w. Liu, K. Zhang and C.-z. Li, *New Carbon Mater.*, 2015, **30**, 349–356.
65 Q. Wang, S. Li, S. Pan, X. Cui, D. J. Corr and S. P. Shah, *Constr. Build. Mater.*, 2019, **198**, 106–119.
66 M. Jin, L. Jiang and Q. Zhu, *Constr. Build. Mater.*, 2017, **143**, 1–15.
67 S. Bykkam, V. Rao, S. Chakra and T. Thunugunta, *J. Adv. Res*, 2013, **4**, 1005–1009.
68 G. Li, J. B. Yuan, Y. H. Zhang, N. Zhang and K. M. Liew, *Composites, Part A*, 2018, **114**, 188–195.
69 S. H. Lv, L. J. Deng, W. Q. Yang, Q. F. Zhou and Y. Y. Cui, *Cem. Concr. Compos.*, 2016, **66**, 1–9.
70 W.-J. Long, J.-J. Wei, F. Xing and K. H. Khayat, *Cem. Concr. Compos.*, 2018, **93**, 127–139.
71 S. Lv, Y. Ma, C. Qiu, T. Sun, J. Liu and Q. Zhou, *Constr. Build. Mater.*, 2013, **49**, 121–127.
72 K. Chintalapudi and R. M. R. Pannem, *J. Build. Eng.*, 2020, **32**, 101551–101561.
73 K. Chintalapudi and R. M. Rao Pannem, *Mater. Today: Proc.*, 2021, **45**, 3971–3975.
74 S. Sharma, N. C. Kothiyal and M. Chitkara, *RSC Adv.*, 2016, **6**, 103993–104009.
75 Y. Xu, *Ceramics*, 2020, 310–319, DOI: **10.13168/cs.2020.0020**.

© 2022 The Author(s). Published by the Royal Society of Chemistry